



Fast response temperature sensor based on reduced graphene oxide through electron beam direct writing

Luzhen Hao^a, Xue Xiao^a, Yanan Wu^{a,b}, Kaimin Zhang^a, Rui Li^a, Hao Tian^a, Yanqing Ma^{a,b,c,*}, Lei Ma^{a,b,*}

^a Tianjin International Center for Nanoparticles and Nanosystems, Tianjin University, Tianjin 300072, PR China

^b Tianjin Key Laboratory of Low-dimensional Electronic Materials and Advanced Instrumentation, Tianjin 300072, PR China

^c School of Precision Instrument and Opto-electronics Engineering, Tianjin University, Tianjin 300072, PR China

ARTICLE INFO

Keywords:

Temperature sensors
Graphene oxide
Electron beam reduction
Carbon materials
Fast response

ABSTRACT

In this work, a thorough investigation of electron beams induced graphene oxide reduction has been conducted. A highly sensitive graphene-based temperature sensor had been proposed by using electron beam reduction of graphene oxide (GO) as a temperature-sensitive layer. It had a resistance temperature coefficient (TCR) of 1.18 %/°C and a response time of 0.17 s in the temperature range of 30 °C ~ 80 °C for the optimized electron beam parameters on rGO production. The effect of electron beam dose dependence on the performance of temperature sensors has been systematically investigated. These results showed that the temperature sensors fabricated by this method had high sensitivity, fast response time, good linearity and low hysteresis. Furthermore, the transport mechanism of the temperature sensor was revealed.

1. Introduction

Owing to the high stability, rapid response and simplicity in fabrication, high-precision resistive temperature sensors are playing an important role in daily life [1]. Nevertheless, conventional used channel materials such as platinum have severely limited their development due to the high price and the low initial resistance [2]. As a very promising substitution of conventional materials, the reduced graphene oxides (rGO) have attracted extensive attention in past decades [3–6] due to their ultimate surface-volume ratio and large varies of optional surface chemical properties upon the synthesis methods. Rooting from graphene oxide (GO), which is an insulator, the resistance of reduced graphene oxide (rGO) varies several orders of magnitude ranging from semiconductor to a graphene-like semimetal [7]. The temperature sensor fabricated by it can exhibit a negative temperature coefficient of resistance (TCR), with a wide operating temperature range as well as high sensitivity [8].

Currently, there is a broad spectrum of methods for preparing temperature sensors using rGO, such as thermal process [8–10], chemical treatments [9–11], and laser reduction [12]. In 2018, Sehrawat et al. [13]. made a rGO temperature sensor by thermal reduction that had a resistance temperature coefficient (TCR) up to 0.801 %/°C and a

response time of 52 s in the temperature range of 30 °C ~ 100 °C. But the thermal reduction method inevitably required high temperature that potentially can be detrimental to other electronic devices which might be integrated to the sensor eventually in practically applications. Sahoo et al. [14] fabricated a fast rGO temperature sensor by using chemical reduction with a response time of 0.59 s and a recovery time of 7.22 s. However, chemical reduction required the usage of highly toxic reductants that could cause serious environment problems [15]. Meanwhile, laser beam reduction of GO (LIG) has been recently developed for realizing single step patterned rGO production [16]. Although this method has shown much superior to those conventional approaches, such as directly patterning without extra post lithograph step needed in order to fabricated patterned rGO, ambient condition operation solely, and high production yield rate, its rather low sensitivity (0.142 %/°C) and tens of micrometer patterned pitch size essentially are barricades for its applications in much broad field [17,18]. As an alternative, electron beam irradiation (EBI) induced rGO as a possibility to upgrade this type of technique in temperature sensors with higher device density and better sensitivity [19,20].

The interaction of high-energy electrons with the material can ionize and energize the molecules, therefore, trigger the chemical reactions [9, 21], consequently, using highly focused electron beams can achieve

* Corresponding authors at: Tianjin International Center for Nanoparticles and Nanosystems, Tianjin University, Tianjin 300072, PR China
E-mail addresses: mayanqing@tju.edu.cn (Y. Ma), lei.ma@tju.edu.cn (L. Ma).

<https://doi.org/10.1016/j.sna.2024.115669>

Received 9 March 2024; Received in revised form 4 June 2024; Accepted 1 July 2024

Available online 2 July 2024

0924-4247/© 2024 Elsevier B.V. All rights are reserved, including those for text and data mining, AI training, and similar technologies.

micrometer or even nanometer sized reduction of graphene oxides [9, 20]. More often, certain processes that are not possible with thermal or optical treatments can be accomplished with electron beam irradiation. As the most promising nanoscale rGO fabrication approach, it is non-toxicity, chemical-free and highly efficient [20,22] with high tunability. However, the research on both the technique and mechanism of EBI based graphene oxide reduction just begins [15].

Here, we present a systematic investigation on the electron beam reduced GO with different electron beam doses and beam energies. It was found that the TCR decreases with the increase of electron beam dose monotonically ranging from 1.34 %/°C to 0.59 %/°C in the temperature range of 30 °C ~ 80 °C. Upon these results, rGO based temperature sensors were made, excellent TCR value of 1.18 %/°C, and the response time was only 0.17 s was realized. Compared with the rGO temperature sensors obtained by other methods, the rGO temperature sensors which was fabricated through EBI technique have much wider range of TCR variation and shorter response time.

2. Materials preparation and device fabrication

GO was prepared using the modified Hummers [23] oxidation method, detailed information could be found in the supplementary information. In order to characterize the defect density of electron beam irradiated GO, the confocal Raman spectrometer (RTS-2, Titan Electro-Optics (Hong Kong) Co Ltd) with a laser wavelength of 532 nm was used. The defect density of rGO was quantitatively characterized by analyzing the peak intensity ratios of the D peak (~1350 cm⁻¹) and the G peak (~1580 cm⁻¹) [13,24]. As shown in Fig. 1a, the Raman mappings of GO that reduced at different electron beam doses (10, 500, 5000, 10000 mA·s/cm²) showed that the I_D/I_G decreases with the increases of the electron beam dose, and at the dose of 10,000 mA·s/cm², the I_D/I_G was ~ 0.81. Fig. 1b corresponds to the Raman spectra under the above electron beam irradiation doses. As the degree of reduction increases, the defects in rGO continue to decrease, resulting in a more ordered sample, which was consistent with studies in the literature [13].

The sensor fabrication procedure was shown in Fig. 2a, where the two metal electrodes with 10 μm space were patterned as external terminals on SiO₂/Si substrate. Firstly, the substrates were hydrophilized using RIE and hung with hydroxylated. Then, GO DI water solvent with a concentration of 2.7 mg/ml was spin-coated over the gaps. Before being used, the GO solution was ultrasonicated at a frequency of 40 kHz for 1 h. The thickness of GO films was controlled to be around 10 nm by multiple times spin-coating. Finally, the EBI was applied to the GO between the two electrodes by using an electron beam lithography instrument (TESCAN VEGA3) at an accelerating voltage of 15 KV (Other

acceleration voltages were shown in the Supporting Information Fig.S1) and beam current of I_{BC} ~ 1.59 nA. The finished device was shown in the inset of Fig. 2a.

In this work, the sample was placed on a heating pad and heated by energizing the pad. The device was connected to a 2450 signaling meter to monitor the real-time resistance of the sample (50 % RH humidity in atmospheric conditions). Current–Voltage (I–V) characteristics of the sensors were conducted to measure the conductance change of rGO films with different electron beam doses of 10, 500, 5000, and 10,000 mA·s/cm², which was shown in Fig. 2b. The linearity of measured I–V curves indicated the nice ohmic contacts between GO and relevant metal leads [25]. Moreover, with the increase of the electron beam dose, the resistance of rGO film decreased. This was due to the reduction of oxygen-containing functional groups on the surface of GO through the increase of the exposing dose, which leads to large recovery of sp² hybrid orbitals, therefore, the enhancement of its electrical conductivity. These results demonstrated that as the exposing dose increasing, the resistance of the reduction area became smaller and GO reduction was more complete.

3. Performance test of fabricated temperature sensors

GOs with different extents of reduction were used as a temperature sensitive layer for the fabrication of temperature sensors and their performance were measured. Temperature coefficient of resistance (TCR), response time, and thermal hysteresis (H_{th}) are the three most important parameters in temperature sensors [17]. We investigated the above three sensing properties of rGO temperature sensors that were fabricated at different electron beam doses.

3.1. Temperature resistance coefficient (TCR)

As shown in Fig. 3a and b, the resistance-temperature curves of the reduced GO-prepared temperature sensors were investigated with electron beam doses of 10 and 20 mA·s/cm². Thermal hysteresis was calculated from the resistance-temperature fitting curve, as shown in the upper right inset (resistance-temperature curves for other electron beam doses were shown in the Supporting Information Fig.S2). The inverse proportion relation between the resistance and temperature indicated its negative temperature coefficient, which could be attributed to features of semiconductor [26,27]. The high defects rGO result in a thin barrier layer for charge carrier transfer, as the temperature rises, the probability of carriers crossing the barrier will increase significantly as well as the carrier tunneling effect between neighboring rGO layers. Consequently, the carrier mobility of rGO largely increases with the rise of

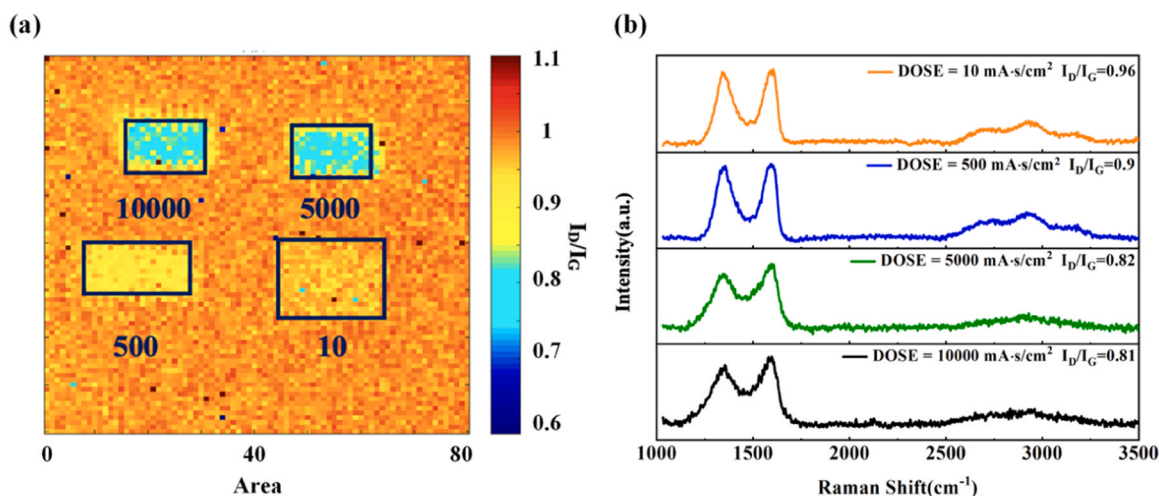


Fig. 1. (a) Raman mapping and (b) Raman spectra of reduced GO with electron beam doses of 10, 500, 5000, and 10000 mA·s/cm².

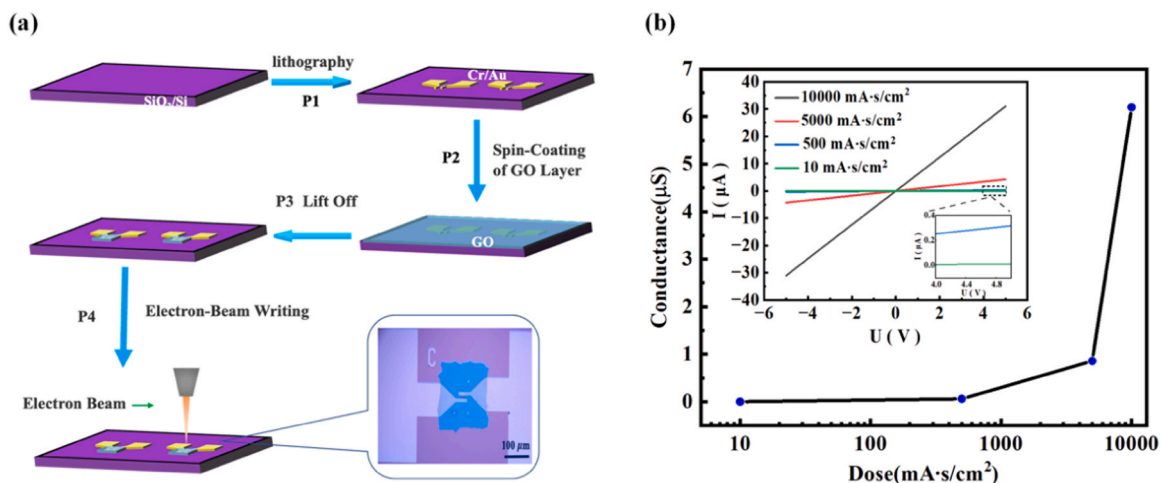


Fig. 2. (a) Schematic diagram of temperature sensor preparation. (b) Conductance of EBIGO as a function of electron beam dose. The insert plots in (b) exhibit the I-V curves at different electron beam doses.

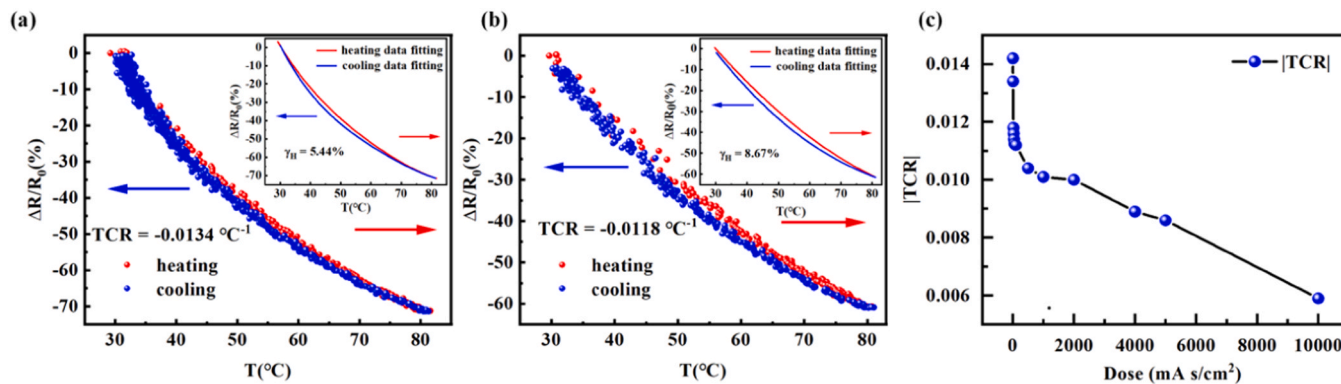


Fig. 3. Resistance-temperature relationship curves of temperature sensors fabricated by reduced GO at electron beam doses of (a) 10 and (b) 20 mA·s/cm², and the inset plots exhibited the thermal hysteresis calculated from the resistance-temperature fitting curves. (c) TCR value of the temperature sensor as a function of electron beam dose.

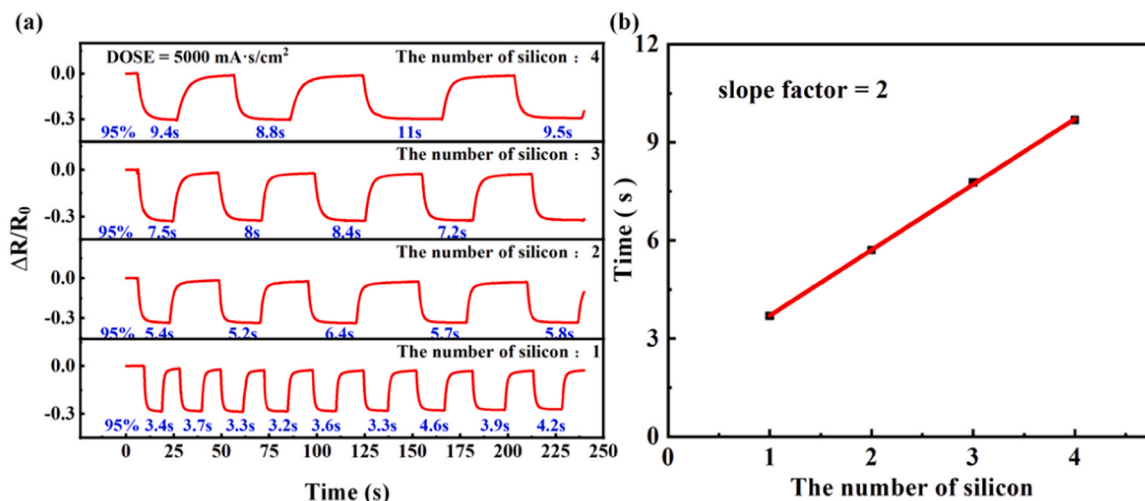


Fig. 4. (a) Response times of temperature sensors prepared at a dose of 5000 mA·s/cm² and tested with temperature-sensitive layers placed on 1, 2, 3, and 4 layers of silicon wafers, respectively. (b) Response time of the temperature sensor as a function of the number of silicon wafers. Its slope is 2, indicating an additional response time of 2 seconds for a single substrate.

temperature, leading to the decrease of its resistivity [26]. The responsiveness of the device can be calculated by following Eq. (1) as

$$\frac{(R_t - R_0)/R_0}{T_t - T_0} \times 100\% \quad (1)$$

where R_t and R_0 are the resistances at temperature T_t and the initial temperature T_0 , respectively [27,28]. The TCRs of the temperature sensors were summarized in Fig. 3c as a function of different electron beam doses (10, 20, 30, 40, 60, 100, 500, 1000, 2000, 4000, 5000, 10000 mA·s/cm²). Experimental results showed that the smaller the electron beam doses, the larger the TCRs. However, for pure GO, the resistance shows no temperature dependence. The minimum dose with nonzero measured TCR is 10 mA·s/cm², which has the maximum TCR about 1.34 %/°C in the temperature range of 30 °C ~ 80 °C. This can be interpreted as diminish of rGO defects with the enhancement of reduction of GO, consequently, leading to a lower responsiveness to temperature [27,29]. It is further verified by the Raman measurements.

3.2. Response time

The functional material layer was spin-coated on the substrate, and response time measurements with the consideration of the elongation caused by silicon wafers substrate since its finite heat transfer speed. Fig. 4a showed the time response property of temperature sensor prepared at the dose of 5000 mA·s/cm² (from room temperature to 50 °C (~24–50 °C) in 240 s). Fig. 4b showed the same sensor but with the number of silicon substrates, the slope indicated that actual device response delay caused by the substrate was 2 s.

Subsequently, we also investigated the beam dose dependent response time of the sensors which are presented in Fig. S3. Fig. 5a exhibited the dynamic response curve at a dose of 20 mA·s/cm², and Fig. 5b showed that on a single wafer, the response time of the sensor was about 2.17 s and the recovery time was about 2.45 s. Considering the delay resulted by the silicon substrate, the actual response time of the temperature-sensitive layer was only 0.17 s. It was much shorter than the reduction GO based temperature sensors by other methods.

3.3. Thermal hysteresis (H_{th})

Another important problem of temperature sensors is thermal hysteresis (H_{th}). Thermal hysteresis refers to the phenomenon that the sensor's resistance is different during warming up and cooling down to the same temperature, and hysteresis is one of main reason cause the

measurement error. Since GO is a hydrophilic material, and its resistance is sensitive to humidity. The water remaining in GO after spin-coating with the water absorbed under atmospheric conditions have a great influence on its thermal hysteresis. We found that thermal hysteresis can be largely decreased by baking the device in an oven at 50 °C for 12 h before testing. As shown in Fig. 6a and b, the thermal hysteresis of the temperature sensor (with the dose of 60 mA·s/cm²) after baking can be reduced from 8.36 % to 3.20 %, which means that the corresponding measured temperature error decrease from 4.2 °C to 1.6 °C in the temperature range of 30 °C – 80 °C. As shown in Fig. 6c and d, they are the resistance-temperature tests without and with baking, respectively. Without baking, after 20 heating and cooling cycling the curves show significantly downward shift, while with baking the 1st and 20th cycling curves nearly perfect overlapping in the temperature range of 30 °C – 50 °C.

4. Transport properties analysis

For rGO based devices, in addition to electron-phonon scattering, the energy dissipation of charge carriers resulted by defects, impurities, edges, and rGO/metal electrode interfaces play very important roles [30,31]. As a type of particulate film and the resistance showing negatively correlated dependence on the temperature [32], so its transport properties can be rationally described using as following Eq. (2)

$$R = R_0 \exp(T_0/T)^p \quad (2)$$

where R_0 is the pre-factor and T_0 is the characteristic Mott temperature associated with the energy required for carrier hopping, $p = 1/(D+1)$ and D is the dimension of the system which is the index to distinguish different mechanisms. The transport behavior dominated by 2D Mott-VRH (variable range hopping) with exponent $p = 1/3$; 3D Mott-VRH with exponent $p = 1/4$; 2D Efros Shklovskii-VRH with exponent $p = 1/2$; and for thermally activated Arrhenius transport mechanisms applicable to higher temperature intervals, exponent $p = 1$ [33,34]. Moreover, the Resistance Curve Derivative Analysis (RCDA) [35] is a highly effective methods for the determination of p . p can be obtained from the slopes of $\ln w$ and $\ln T$, where the w and p can be extracted as following Eqs. (3) and (4)

$$w = \frac{d(\ln R)}{d(\ln T)} \quad (3)$$

$$p = -\frac{d(\ln w)}{d(\ln T)} \quad (4)$$

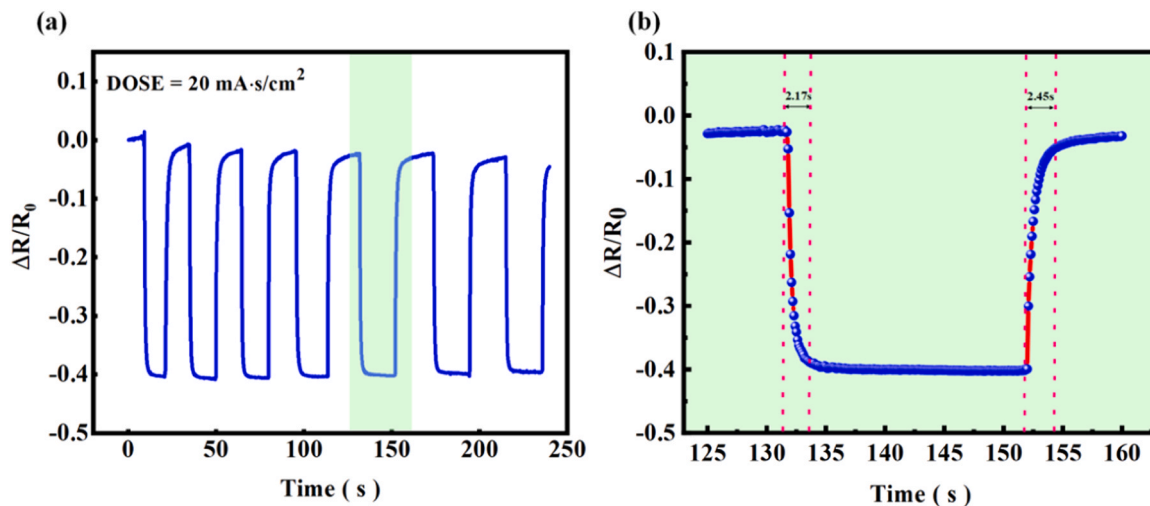


Fig. 5. (a) Measured response time of a temperature sensor prepared at the dose of 20 mA·s/cm² on a single silicon wafer. (b) The response time was about 2.17 s and the recovery time was about 2.45 seconds.

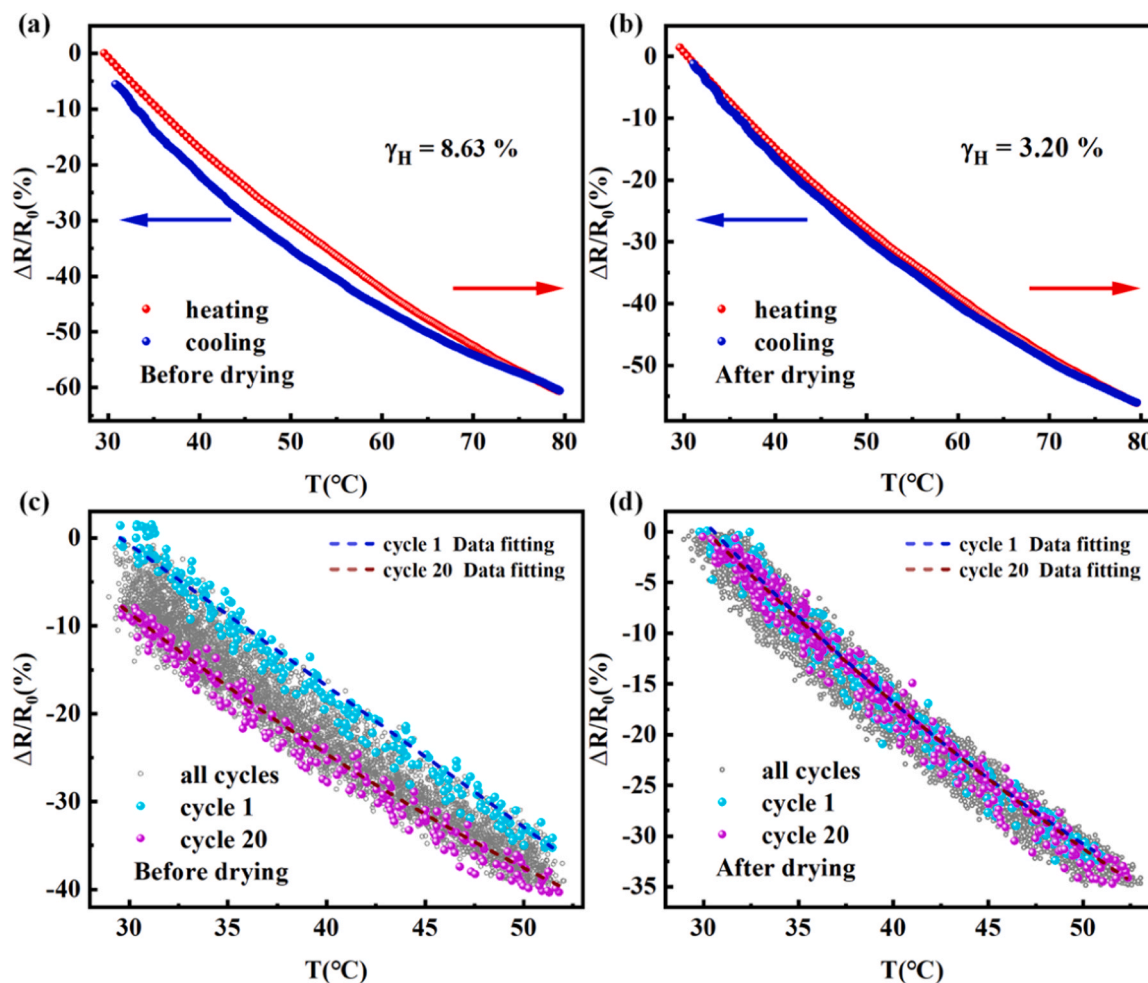


Fig. 6. (a)(b) The resistance temperature tested before and after drying, respectively. Thermal hysteresis can be reduced from 8.36 % to 3.20 % before and after drying in the temperature range of 30 °C~80 °C. (c)(d) Resistance temperature curves for 20 sequential cycles of testing, before and after drying in the temperature range of 30 °C~50 °C.

As shown in Fig. 7a, the slopes of the $\ln w - \ln T$ change at about 330 K. The slopes of the calculated $\ln w(\ln T)$ in the range of 150 K to 330 K are shown in Fig. 7b, which is -0.26 with a p-value of about $\frac{1}{4}$ and indicating that 3D Mott-VRH. The temperature resistance dependence of the characteristic at 150–330 K is shown in Fig. 7c. Substituting $p=1/4$ into Eq. (2) in the inset plot results in a linear relationship between $\ln R$ and $T^{-1/4}$. Hence, the temperature dependence of the electrical transport properties of MEB-rGO thin film materials in the temperature range of 150 K~330 K satisfies ideally the Mott 3D-VRH transport.

Above 330 K in Fig. 7a, there was a change in the slope of the differential resistance curve ($p=1$), reflecting the change of dominant transport, which was no longer a VRH, and the detailed study of the transport mechanism of rGO thin films has been investigated by Negishi et al. [36,37]. The VRH behavior suggested the existence of localized electronic states near the Fermi energy level [33]. As the temperature increases, the electrons gain sufficient energy and leap from the states below the Fermi energy to above, consequently transitioning to thermally excitation-dominated transport (Arrhenius transport mechanism) regime [38–40]. As shown in Fig. 7d, the temperature resistance dependence characteristics at 330–375 K. Substituting $p=1$ into Eq. (2), a linear relationship between $\ln R$ and T^{-1} fitting was obtained. The Arrhenius transport mechanism of MEB-rGO thin film materials in the temperature range of 330 K~375 K was demonstrated.

5. Conclusion

In this work, a temperature sensor with high sensitivity and fast response was fabricated by using a novel electron-beam direct-write method of patterned reduction of GO. The effect of electron beam dose on the sensitivity of temperature sensors was systematically investigated and the materials were characterized by both Raman and electrical transport measurement. It was found that the TCR decreased with increasing electron beam dose and could be varied from 1.34 %/°C to 0.59 %/°C in the temperature range of 30 °C ~ 80 °C, and the prepared sensor exhibited the highest sensitivity (~ 1.18 %/°C), the fastest response time (~ 0.17 s) as well as a superior linearity at an electron beam dose of 20 mA/cm². Moreover, the humidity had a large effect on the hysteresis of the rGO temperature sensor, and the thermal hysteresis could be reduced from 8.36 % to 3.20 % by simple baking. The results also showed an interesting mechanism transition at temperature about 330 K from 3D Mott-VRH to thermally activated Arrhenius. The research was compatible with current silicon-based techniques and provided a new way to monitor overheating in electronic devices.

CRedit authorship contribution statement

Luzhen Hao: Writing - original draft, Investigation, Conceptualization. **Xue Xiao:** Visualization, Data curation, Conceptualization. **Yanan Wu:** Methodology, Data curation. **Kaimin Zhang:** Methodology, Data curation. **Rui Li:** Methodology, Data curation. **Hao Tian:** Visualization,

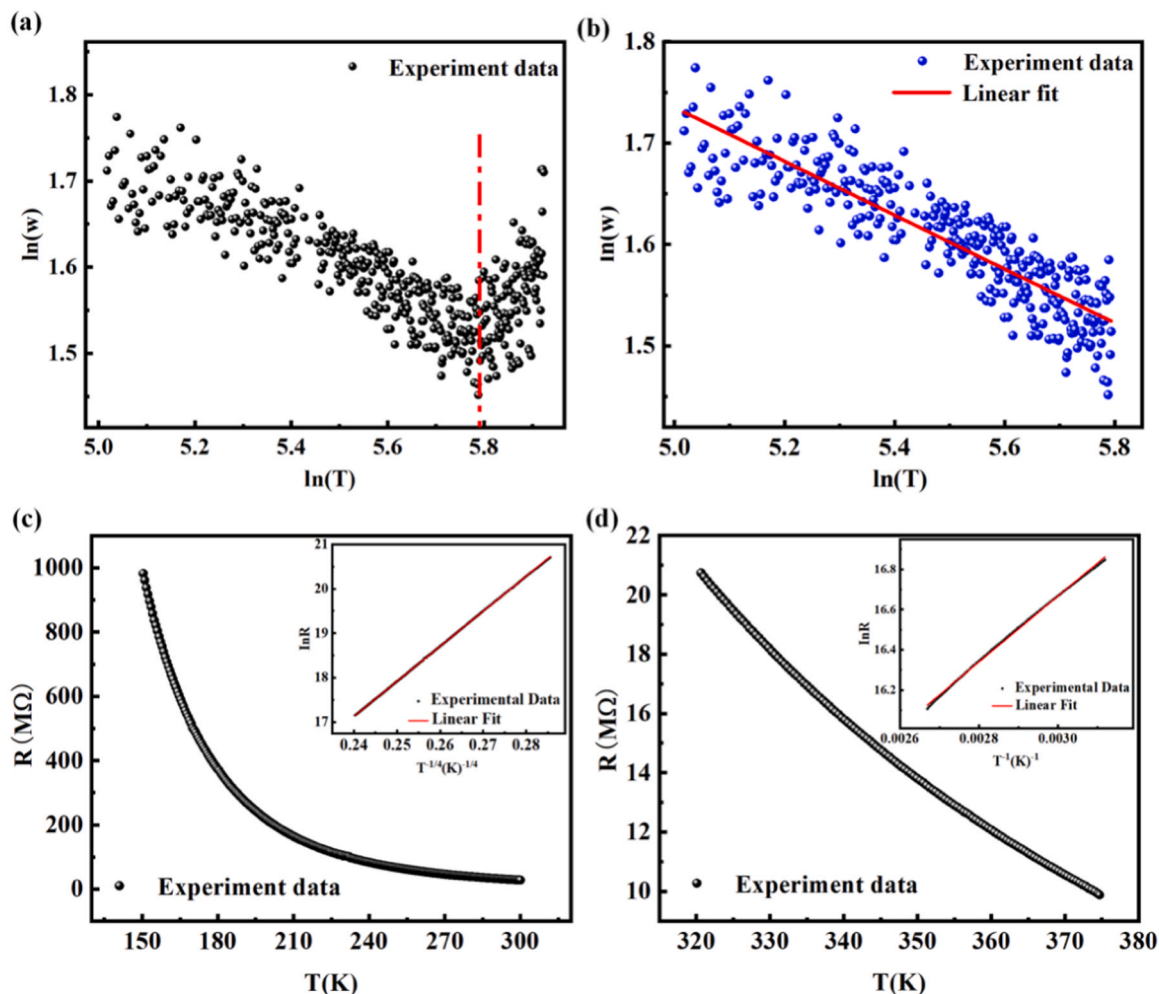


Fig. 7. (a) Resistance Curve Derivative Analysis (RCDA) Plot in the temperature interval 150 K~375 K. (b) Slope fit of the RCDA plot in the temperature interval 150 K~330 K for $p=1/4$. (c) Temperature resistance dependent characterization at 150–330 K, inset for $\ln R$ as a function of $T^{-1/4}$. (d) Temperature resistance dependent characterization at 330–375 K, inset for $\ln R$ as a function of T^{-1} .

Formal analysis. **Yanqing Ma:** Writing - review & editing, Supervision, Project administration, Conceptualization. **Lei Ma:** Writing - review & editing, Supervision, Funding acquisition, Conceptualization.

Declaration of Competing Interest

The authors declare that they have no known competing financial interests or personal relationships that could have appeared to influence the work reported in this paper.

Data availability

Data will be made available on request.

Acknowledgments

This work was financially supported by the National Key R&D Program of China (No. 2022YFC3006303).

Appendix A. Supporting information

Supplementary data associated with this article can be found in the online version at [doi:10.1016/j.sna.2024.115669](https://doi.org/10.1016/j.sna.2024.115669).

References

- [1] B.A. Kuzubasoglu, et al., Flexible temperature sensors: a review, *Sens. Actuators A* 315 (2020) 112282.
- [2] G.C.M. Meijer, et al., Smart temperature sensors and temperature sensor systems, *Smart Sens. MEMS* (2018) 57–85.
- [3] C. Berger, et al., Epigraphene: epitaxial graphene on silicon carbide, *MRS Bull.* 35 (04) (2010).
- [4] F. Ming, et al., A model for the epitaxial growth of graphene on 6H-SiC, *Phys. Rev. B* 84 (2011) 115459.
- [5] H. Yang, et al., Correlation between molecular structure and interfacial properties of edge or basal plane modified graphene oxide, *ACS Appl. Nano Mater.* 1 (2018) 2763–2773.
- [6] F. Li, et al., Graphene oxide: A promising nanomaterial for energy and environmental applications, *Nano Energy* 16 (2015) 488–515.
- [7] D. Chen, et al., Graphene oxide: Preparation, functionalization, and electrochemical applications, *Chem. Rev.* 112 (2012) 6027–6053.
- [8] S. Pei, et al., The reduction of graphene oxide, *Carbon* 50 (2012) 3210–3228.
- [9] P. Gullia, et al., Synthesis of graphene oxide thin film and effect of electron beam irradiation, *AIP Conf. Proc.* 1832 (2017) 140023.
- [10] Z.S. Wu, et al., Synthesis of high-quality graphene with a pre-determined number of layers, *Carbon* 47 (2009) 493–499.
- [11] S. Stankovich, et al., Synthesis of graphene-based nanosheets via chemical reduction of exfoliated graphite oxide, *Carbon* 45 (2007) 1558–1565.
- [12] C.R. Yang, et al., Laser-induced reduction of graphene oxide powders by high pulsed ultraviolet laser irradiations, *Appl. Surf. Sci.* 444 (2018) 578–583.
- [13] P. Sehrawat, et al., Reduced graphene oxide based temperature sensor: Extraordinary performance governed by lattice dynamics assisted carrier transport, *Sens Actuators B Chem.* 258 (2018) 424–435.
- [14] S. Sahoo, et al., Reduced graphene oxide as ultra fast temperature sensor, *ECS Meet. Abstr.* (50) (2012).
- [15] K.H. Wu, et al., Electron-beam writing of deoxygenated micro-patterns on graphene oxide film, *Carbon* 95 (2015) 738–745.

- [16] J.L. Li, et al., One-step synthesis of Co_3O_4 nanoparticles/laser induced graphene composites in ambient condition for electrocatalytic OER reaction, *Carbon Trends* 12 (2023) 100285.
- [17] R. Chen, et al., Facile fabrication of a fast-response flexible temperature sensor via laser reduced graphene oxide for contactless human-machine interface, *Carbon* 187 (2022) 35–46.
- [18] S. Gandla, et al., Highly linear and stable flexible temperature sensors based on laser-induced carbonization of polyimide substrates for personal mobile monitoring, *Adv. Mater. Technol.* 5 (2020) 2000014.
- [19] P. Kumar, et al., Graphene patterning and lithography employing laser/electron-beam reduced graphene oxide and hydrogenated graphene, *Mater. Express* 1 (2011) 252–256.
- [20] S. Kim, et al., Localized conductive patterning via focused electron beam reduction of graphene oxide, *Appl. Phys. Lett.* 106 (2015), 133109-1.
- [21] O.O. Kapitanova, et al., Direct patterning of reduced graphene oxide/graphene oxide memristive heterostructures by electron-beam irradiation, *J. Mater. Sci. Technol.* 38 (2020) 237–243.
- [22] J. Liu, et al., Nanoresolution patterning of hydrogenated graphene by electron beam induced C-H dissociation, *Nanotechnology* 29 (2018).
- [23] J. Chen, et al., An improved Hummers method for eco-friendly synthesis of graphene oxide, *Carbon* 64 (2013) 225–229.
- [24] M.A. Pimenta, et al., Studying disorder in graphite-based systems by Raman spectroscopy, *Phys. Chem. Chem. Phys.* 9 (2007) 1276–1291.
- [25] P. Sehwat, et al., Spectroscopic analysis of multi-walled carbon nanotube-alumina composite films: optimization of temperature coefficient of resistance and thermal hysteresis for thermal sensor applications, *Mater. Sci. Semicond. Process* 31 (2015) 116–123.
- [26] Rahaman, A. Bin, et al., Observation of different charge transport processes and origin of magnetism in rGO and rGO-ZnSe composite, *J. Phys. Chem. C* 123 (2019) 15441–15450.
- [27] R. Han, et al., Facile fabrication of rGO/LIG-based temperature sensor with high sensitivity, *Mater. Lett.* 304 (2021).
- [28] Q. Liu, et al., A high-performance flexible temperature sensor composed of polyethyleneimine/reduced graphene oxide bilayer for real-time monitoring, *Adv. Mater. Technol.* 4 (2019) 1800594.
- [29] T.Q. Trung, et al., A stretchable strain-insensitive temperature sensor based on free-standing elastomeric composite fibers for on-body monitoring of skin temperature, *ACS Appl. Mater. Interfaces* 11 (2019) 2317–2327.
- [30] A.A. Balandin, et al., Thermal properties of graphene and nanostructured carbon materials, *Nat. Mater.* 10 (2011) 569–581.
- [31] S. Ghosh, et al., Extremely high thermal conductivity of graphene: prospects for thermal management applications in nanoelectronic circuits, *Appl. Phys. Lett.* 92 (2008) 151911.
- [32] Fei Zheng, et al., Charge transfer from poly(3-hexylthiophene) to graphene oxide and reduced graphene oxide, *RSC Adv.* 5 (2015) 89515.
- [33] A.B. Rahaman, et al., Observation of different charge transport processes and origin of magnetism in rGO and rGO-ZnSe composite, *J. Phys. Chem. C* 123 (2019) 15441–15450.
- [34] D. Joung, et al., Efros-Shklovskii variable-range hopping in reduced graphene oxide sheets of varying carbon sp^2 fraction, *Phys. Rev. B* 86 (2012) 235423.
- [35] S.M. Jilani, et al., Graphene oxide–zinc oxide nanocomposite as channel layer for field effect transistors: effect of ZnO loading on field effect transport, *ACS Appl. Mater. Interfaces* 6 (2014) 16941–16948.
- [36] W.J. Park, et al., Electrical and thermal conductivities of reduced graphene oxide/polystyrene composites, *Appl. Phys. Lett.* 104 (2014) 113101.
- [37] A. Vianelli, et al., Observation of different charge transport regimes and large magnetoresistance in graphene oxide layers, *Carbon* 89 (2015) 188–196.
- [38] R. Negishi, et al., Band-like transport in highly crystalline graphene films from defective graphene oxides, *Sci. Rep.* 6 (2016) 28936.
- [39] I. Jung, et al., Tunable electrical conductivity of individual graphene oxide sheets reduced at “low” temperatures, *Nano Lett.* 8 (2008) 4283–4287.
- [40] G. Venugopal, et al., An investigation of the electrical transport properties of graphene-oxide thin films, *Mater. Chem. Phys.* 132 (2012) 29–33.

Luzhen Hao received her B.S. degree from Hebei Normal University in 2019. She is currently working toward the Ph.D degree in Physics with Tianjin International Center for Nanoparticles and Nanosystems, Tianjin University. Her current research interest is graphene-gallium nitride composite electronics devices.

Xue Xiao received her M.S. degree from Tianjin International Center for Nanoparticles and Nanosystems, Tianjin University in 2023. Her project is devoted to research graphene-based ammonia sensors for the early diagnosis of diseases.

Yanan Wu received her Ph.D degree in material physics and chemistry from Tianjin University in 2014. She joined the International Center for Nanoparticles and Nanosystems in Tianjin University in 2016. Her research focuses on the quantum transport properties of two-dimensional nanomaterials.

Kaimin Zhang received her B.S. degree from North China University of Water Resources and Electric Power in 2016. She is currently working toward the Ph.D. degree in materialogy with Tianjin International Center for Nanoparticles and Nanosystems, Tianjin university. Her current research interest is developing quantum chips for computers.

Rui Li graduated from Nanjing University of Technology with a Bachelor’s degree in Engineering in 2017. He is currently pursuing a doctoral degree in Materials Science at the Tianjin International Center for Nanoparticles and Nanosystems at Tianjin University. His current main research is the development of graphene based all carbon devices and functional circuits.

Hao Tian received his bachelor’s degree from Hefei University of Technology in 2020 and his master’s degree from Tianjin University in 2023. He is currently pursuing a doctoral degree in instrument science and technology with Tianjin International Center for Nanoparticles and Nanosystems at Tianjin university. His current research interest is the graphene based device and circuits.

Yanqing Ma received her Ph.D. in physical chemistry from Lanzhou Institute of Chemical Physics, CAS in 2009. She joined the International Center for Nanoparticles and Nanosystems in Tianjin University in 2017. Her research focuses on the graphene based energy storage devices and sensors.

Lei Ma received his Ph.D in condensed matter physics in Nanjing University and University of Freiburg in 2009. Then he worked as a postdoctoral researcher at Brown University and Georgia Institute of Technology. In 2015, he joined the faculty to Tianjin University as a Professor and built Tianjin International Center for Nanoparticles and Nanosystems. His current research focuses on the cluster physics, graphene electronics, chemistry, low dimensional condensed matter and their applications on energy materials and devices.